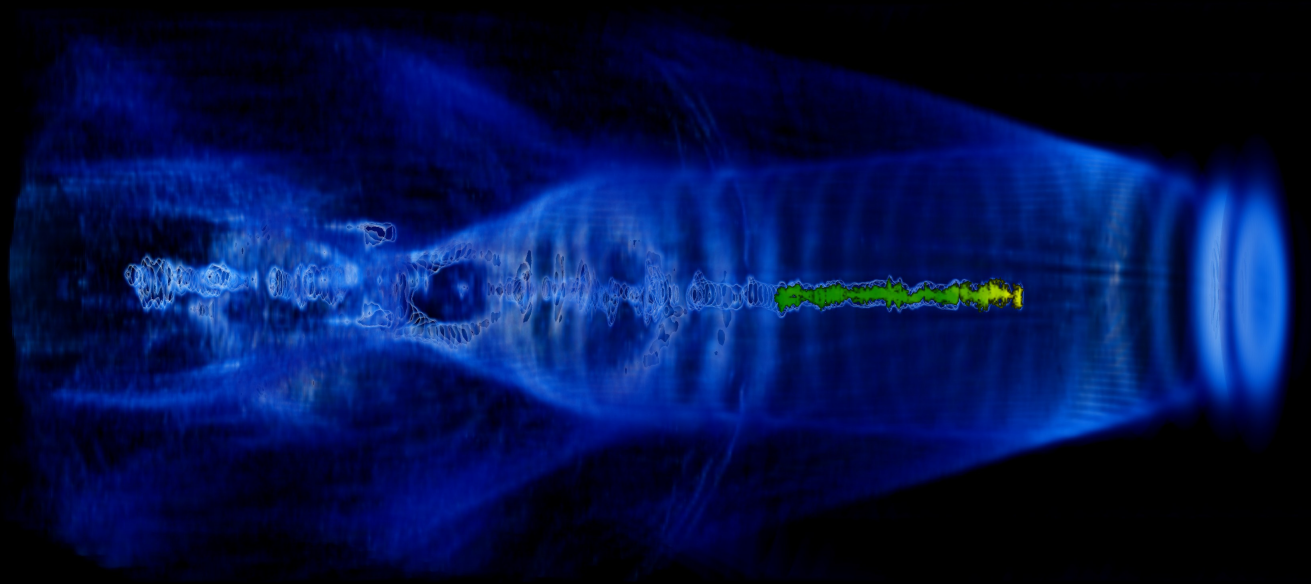


MASTER'S THESIS 2019

# A compact plasma beam dump for next generation particle accelerators

OSCAR JAKOBSSON



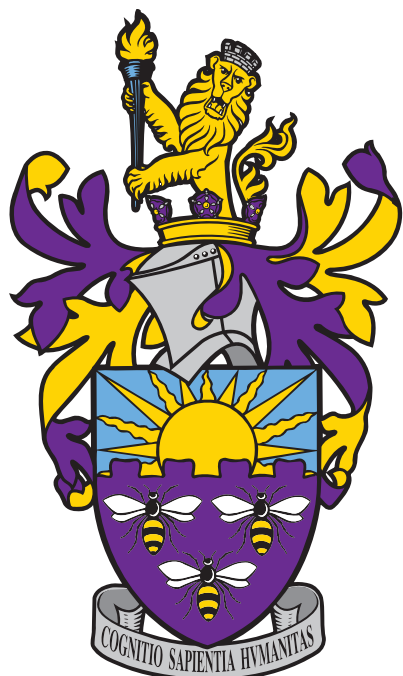
SCHOOL OF PHYSICS AND ASTRONOMY  
THE UNIVERSITY OF MANCHESTER





# A compact plasma beam dump for next generation particle accelerators

OSCAR JAKOBSSON



School of Physics and Astronomy  
*Cockcroft Accelerator Group*  
THE UNIVERSITY OF MANCHESTER  
Manchester, United Kingdom 2019

A compact plasma beam dump for next generation particle accelerators  
OSCAR JAKOBSSON

© OSCAR JAKOBSSON, 2017.

Supervisor: Guoxing Xia, Cockcroft Accelerator Group

Master's Thesis 2019  
School of Physics and Astronomy  
Cockcroft Accelerator Group  
The University of Manchester

Cover: XXX.

Typeset in L<sup>A</sup>T<sub>E</sub>X

A compact plasma beam dump for next generation particle accelerators  
OSCAR JAKOBSSON  
School of Physics and Astronomy  
The University of Manchester

## **Abstract**

Keywords: LWFA, PWFA, collective deceleration, plasma beam dump, EuPRAXIA



## Acknowledgements

Lorem ipsum dolor sit amet, consectetur adipisicing elit, sed do eiusmod tempor incididunt ut labore et dolore magna aliqua. Ut enim ad minim veniam, quis nostrud exercitation ullamco laboris nisi ut aliquip ex ea commodo consequat. Duis aute irure dolor in reprehenderit in voluptate velit esse cillum dolore eu fugiat nulla pariatur. Excepteur sint occaecat cupidatat non proident, sunt in culpa qui officia deserunt mollit anim id est laborum.

Oscar Jakobsson, Manchester, January 2019



# Contents

<b>1</b>	<b>Introduction</b>	<b>1</b>
1.1	Conventional and plasma-wakefield accelerators . . . . .	1
1.2	Beam dumps . . . . .	2
1.3	Outline of report . . . . .	4
<b>2</b>	<b>Simulations</b>	<b>5</b>
2.1	Plasma simulations . . . . .	5
2.2	Particle-in-Cell Codes . . . . .	5
2.3	EPOCH . . . . .	6
2.3.1	Input deck . . . . .	7
2.3.2	Non-analytical bunch initialisation . . . . .	8
<b>3</b>	<b>Theoretical foundations</b>	<b>9</b>
3.1	Introduction . . . . .	9
3.2	Linear fluid model . . . . .	9
3.2.1	Longitudinal accelerating field . . . . .	11
3.2.2	Transverse field . . . . .	15
3.2.3	Plasma deceleration . . . . .	16
<b>4</b>	<b>Simulation tests</b>	<b>17</b>
4.1	Bunch parameters . . . . .	17
4.2	Linear and quasilinear regimes . . . . .	18
<b>5</b>	<b>Current work and concluding remarks</b>	<b>21</b>
<b>6</b>	<b>Conclusion</b>	<b>23</b>
	<b>Bibliography</b>	<b>25</b>

## Contents

---

# 1

## Introduction

### 1.1 Conventional and plasma-wakefield accelerators

Ultra-relativistic electron beams with single-particle energies in excess of a GeV form an integral part of many areas of contemporary science, industry and medicine. For instance, monoenergetic electron bunches allows for the generation of high-quality X-ray pulses through the use of undulators; a technique by which ultra-relativistic electron bunches are rapidly oscillated back-and-forth perpendicular to their direction of propagation [1]. This oscillatory motion can be tuned to generate highly coherent synchrotron radiation in the X-ray spectrum, which can be used in medicine for advanced tissue diagnostics, tomography and radiotherapy cancer treatments [2]. Operating at higher energies, the 1.7 km long European X-ray free electron laser (XFEL) facility in Hamburg, Germany, employs 17.5 GeV electron bunches to generate extremely intense femtosecond X-ray pulses which are used for fundamental research into the structure of materials, biological molecules and even to generate movies of molecular reactions [1]. Probing even smaller length scales takes us into the realm of high-energy electron-positron collider physics, where the size of accelerators grows accordingly. From the 3.2 km long, 45 GeV, SLAC Linear collider (SLC) at Stanford to the decommissioned 27 km long, 105 GeV, Large Electron Positron collider (LEP) at CERN, the fine details of the smallest constituents of our theories are being explored through tests of the standard model of particle physics. Even higher energy electron-positron colliders such as the proposed 50 km long International Linear Collider (ILC) aims to achieve single-particle energies up to 500 GeV. The reason for these progressively larger accelerators stems in part from the reliance on resonant radiofrequency (RF) cavities in order to accelerate particles, which are currently limited to sustaining electric fields no larger than 100MV/m, beyond which point further increase is hampered by material breakdown of the inner walls of the cavity [3]. As the demand for high-energy particle accelerators grows in medicine, industry and fundamental research, the size and cost of accelerators is and will continue to be a limit factor to future progress if no other means of acceleration is developed.

Several novel accelerators techniques currently exists in various stages of development. The most widespread of these is based on the phenomena of *plasma wakefield acceleration*. An ultra-relativistic particle beam or a high intensity laser pulses driven through a pre-formed plasma can excite plasma waves with phase velocities equal to the group velocity of the particle or laser driver [4]. These waves, or 'wakefields', are large-amplitude oscillations of the plasma-electron density which are able to support accelerating electric fields of hundreds of GV/m; thousands of times higher than conventional RF cavities. By injecting an electron, or positron, bunch behind the driver one can then achieve constant acceleration by effectively letting the particle bunch surf the plasma-electron wave. In this manner, provided a sufficiently powerful driver is available, sizeable energy gains can be achieved over relatively short propagation distances. In fact, this form of plasma acceleration was proposed in 1979 by Tajima and Dawson [5], not only as a viable terrestrial particle accelerator but also as a generation mechanism for ultra-high-energy cosmic rays in the plasma rich environment around newly formed pulsars. At the time of their proposal, however, the lack of sufficiently high intensity lasers was a limit factor in exploring these ideas experimentally [6]. The

development of the chirped-pulse laser amplification techniques in 1985 by Strickland and Mourou [7] gave researchers access to ultrashort high-intensity laser pulses. This opened up the possibility of laser-driven plasma wakefield acceleration (LWFA) and several experiments constructed in the following decade were able to successfully demonstrate LWFA of electrons [8]. Recent experiments, propelled by the rapid development of modern multi-terawatt laser facilities, have demonstrated acceleration of electron bunches in a few centimetres of plasma up to 1, 2 and 4 GeV with relatively small energy spreads [9, 10, 11], making LWFA a serious contender for the construction of compact x-ray free-electron lasers [12]. Progress towards even higher energy gains have been made in the last two decades by the construction of dedicated beam-driven plasma wakefield acceleration (PWFA) facilities. Notably, experiments at the Facility for Advanced Accelerator Experimental Tests (FACET) at Stanford aims to use 20 GeV electron and positron beams to drive wakefields which in turn will accelerate secondary electron or positron bunches to higher energies [13]. Furthermore, the Advanced Proton Driven Plasma Wakefield Acceleration Experiment (AWAKE) recently demonstrated proof-of-principle acceleration of secondary electron bunches up to 2 GeV within plasma wakefields driven by the 400 GeV proton beam from CERN’s Super Proton Synchrotron [14]. These experiments are paving the way towards compact high-energy particle accelerators at GeV energies with great promise to science and industry. One can also imagine a future in which plasma wakefield accelerators are used in high-energy physics, perhaps in conjugation with conventional accelerators as a pre-accelerator or energy booster. Even though the latter is probably decades away, both GeV and TeV accelerators might still be able to benefit from plasma wakefield phenomena. Regardless of the means of acceleration, be it larger conventional accelerators or smaller plasma wakefield accelerators, the ultra-relativistic beams produced will need to be dealt with. The current approach for both small and large accelerators is to dump the energy of the beam.

## 1.2 Beam dumps

When in operation, the energy of the 105 GeV electron and positron beams at the LEP at CERN were dumped by directing them into a 2 m long, 40 cm in diameter, aluminium alloy block [15]. The proposed water-based beam dump for the ILC [16], which is to operate at 500 GeV, is significantly different to its lower energy predecessor at LEP. The increased energy and intensity of the ILC beam makes the extraction of its energy from a solid material beam dumps exceedingly difficult due to the limitations imposed by thermal conduction [16]. By using a tank of water the ILC beam energy can be deposited and removed using a pumping system. However, the high intensity beams will lead to water temperatures in excess of 155°C as well as decomposition of water into hydrogen and oxygen gas. This necessitates a high-pressure vessel and a safe way to remove and store these volatile gases. Furthermore, the beam interaction with the water molecules will create the radioactive nuclei  $^3\text{H}$  and  $^7\text{Be}$ , which demands a waste-water storage tank. The tank itself will also suffer radiation damages, specifically the window through which the beam enters the vessel. A report by Satyamurthy et al. [16] estimates that this window will need to be replaced at periodic intervals and due to the induced radioactivity this will have to be done remotely using robotic technology. Although this technology is widely available in the nuclear industry this whole beam dump is a large and costly affair for the ILC and any future HEP accelerators. Moreover, not only HEP accelerators face this issue, even metallic or concrete beam dumps for MeV to low GeV accelerators lead to radioactivation which must be carefully assessed and adequately shielded for [17, 18].

An alternative approach aims to utilize the unprecedented acceleration gradients from PWFA. This idea, called a passive plasma beam dump, was proposed in 2010 by Wu et al. [19]. They simulated a 500 MeV electron bunch and showed that an energy loss of up to 70% was achievable by propagating 2 mm through a dense plasma, as shown in figure 1.1. Full energy depletion

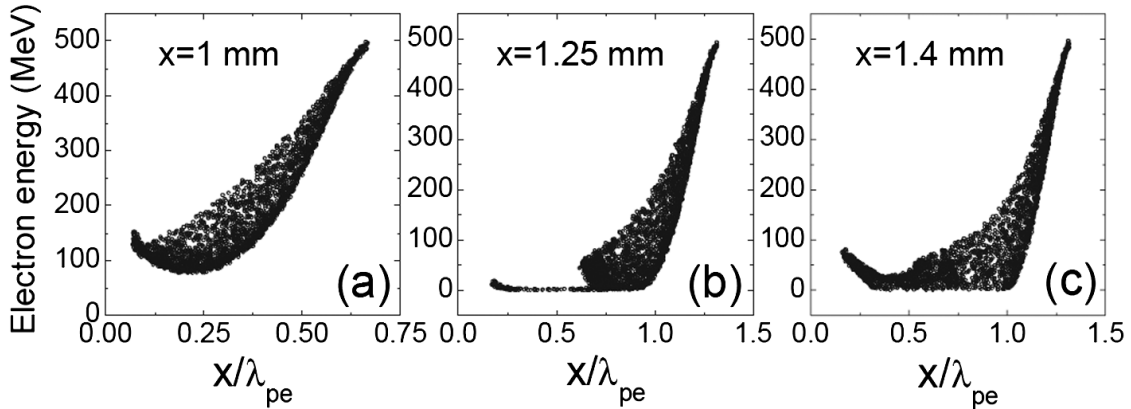


**Figure 1.1:** Energy distributions of an electron bunch during propagation through a dense plasma, as found by Wu et. al [19]. 1(b) shows non-relativistic particles falling behind the head of the bunch and 1(c) shows their subsequently re-acceleration. The x-axis shows the distance along the bunch in relation to the plasma wavelength, which is covered in chapter 3.

was prevented due to decelerated, non-relativistic, electrons falling behind the head of the bunch, figure 1(b), drifting into an accelerating region the wakefield and subsequently re-accelerated to relativistic energies, figure 1(c). This process prevents further significant energy loss and the deceleration is said to have saturated. It was further demonstrated that the decelerating field is independent of the initial bunch energy by demonstrating that a 100 GeV bunch would require 20 cm to loose 70% of its energy [19]. To minimize re-acceleration the simulated plasma was intersected by aerogel foils, strategically placed to capture the non-relativistic particles. This resulted in an energy loss of 90% for the 500 MeV bunch. It is however not clear how prolonged exposure to plasma and interactions with high-energy electron bunches would affect the degradation of these foils. As an alternative, Hanahoe et al. [20] proposed the use of varying plasma density instead of foils. Linear or quadratically increasing plasma densities were shown to achieve comparable reduction of the re-accelerated particles as the foils used by Wu et al. It is however unclear whether such plasma density profiles can be set up and maintained in a plasma cell. Furthermore, the head of the bunch still maintained its energy in both these approaches; this *energy chirp* is evident in figure 1(c) and occurs because the head of the bunch sets up the wakefield but does not experience the decelerating field itself [19]. For the 500 MeV bunch this might not be a major issue since smaller conventional beam dumps could be used to dump this remaining energy. For GeV energies however this energy chirp may still pose an issue due to radioactivation. To address the energy chirp Bonatto et. al [21] proposed the *active beam dump*, whereby a laser pulse is driven ahead of the bunch through a plasma such that a decelerated wakefield is set up around the bunch. By carefully positioning the laser in relation to a 1 GeV bunch it was shown that the energy in the head of the bunch could be significantly reduced, resulting in total energy losses up to 95%. It is however difficult to extend this method to higher energies due to the dispersion of the laser in the plasma, which prevents laser propagation over the longer distances required.

Given that the active approach is able to reduce the energy chirp and that the passive beam dump leaves behind a pronounced energy chirp, the natural continuation of the previous work is to combine these methods. This project endeavours to demonstrate, through simulations, the successful combination of these methods in what we call a *hybrid beam dump*. This scheme is outlined in figure 1.2. The general approach is to use a passive beam dump to decelerate the bunch until saturation and then pass only the head of the bunch through an active beam dump, instead of decelerating the full-energy bunch with a laser driver as in the work by Bonatto et al.. This should have the added benefit of requiring a less powerful laser as well as being applicable to higher

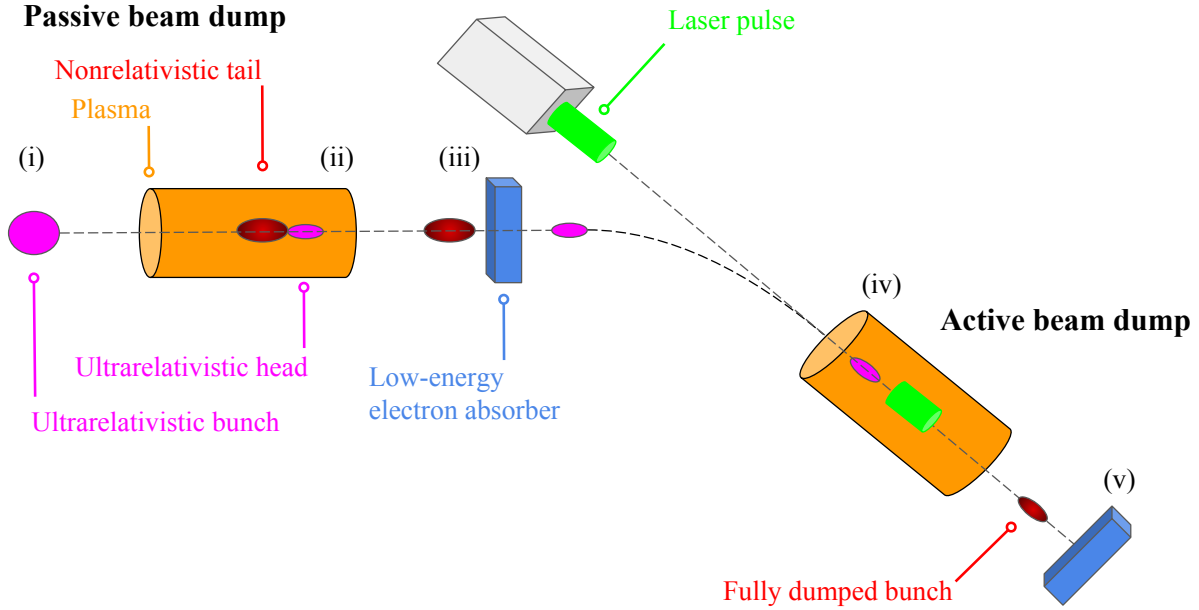


**Figure 1.2:** Outline of the hybrid beam dump scheme at five stages. (i) The incoming ultra-relativistic (violet) electron bunch passes through vacuum towards the first plasma cell. (ii) The electron bunch loses energy as it propagates through the plasma. A non-relativistic (red) tail of particles is formed behind the the head of the bunch, which maintains its energy. (iii) The non-relativistic tail is removed by propagating through an absorbing material and the path of the head is bent by magnets so as to be aligned behind a laser pulse. (iv) The laser pulse drives a plasma wakefield in front of the remaining bunch, decelerating it to non-relativistic energies. (v) The remaining energy is absorbed.

energies since previous work has shown that the energy chirp contains only  $\sim 10\%$  of the initial energy.

### 1.3 Outline of report

This intermediate report details the initial phase of a full-year project on plasma wakefield deceleration and is written in partial fulfilment of the requirements for the degree of Master in Physics. As such, it does not attempt to cover the full scope of the work and research conducted in this project so far, but rather aims to provide an introduction to the field, establish the theoretical background and construct the computational framework necessary to perform the intended research. Having laid the groundwork for the project in this report, the final-year report will reap the rewards of this work by presenting the full results and outcome of the project.

Chapter 2 of this report details the simulation framework used in this project and chapter 3 covers the theory behind beam-driven plasma wakefields. The theory describing laser-driven plasma wakefields, necessary to understand the active beam dump approach, will be covered in a subsequent report. Simulation tests and preliminary results are presented in chapter 4. We conclude this report by summarising the work that has been presented and looking ahead at the work that is to be carried out in the second half of this project.

# 2

## Simulations

### 2.1 Plasma simulations

Numerical simulations are a crucial part of plasma physics research. The accuracy by which modern plasma simulation codes are able to model plasma behaviour allows us to better understand and improve the functioning of our current experiments, as well as to explore and develop new novel ideas without the technological and financial limitations of real-world experiments. As a result, simulation studies play an increasingly more decisive role in guiding and accelerating current plasma wakefield research.

Given that a plasma is, to a good approximation, nothing more than electrons and ions interacting electromagnetically, the response of such a plasma to the propagation of an electron beam or laser pulse could in theory be simulated by solving Maxwell's equations and calculating the Lorentz force law for each electron and ion in the plasma. This approach is however computationally intractable due to vast number of particles present in the simulations we need to perform. We circumvent this computational road block by making use of so-called Particle-In-Cell (PIC) codes. In this chapter we outline the general PIC approach and introduce the plasma physics PIC code EPOCH, which is used throughout this project. We further detail the modifications necessary to allow the hybrid beam dump scheme to be simulated with EPOCH.

### 2.2 Particle-in-Cell Codes

The key feature of all PIC codes is to represent a large ensemble of microscopic particles by a smaller ensamble of macroscopic pseudo-particles on a discrete spatial grid [22]. Each of these macroparticles carries the total charge and mass of the collection of electrons or ions that it represents and, importantly, are not point particles but finite regions of space, 'cells', that move as one. The interactions and dynamical behaviour of these macroparticles is then used as a representation of the actual plasma response. This significantly reduces the computational cost. A further simplifying feature of PIC codes is that the EM fields are only calculated on discrete points on a so-called Yee grid whilst the macroparticles move continuously through this grid, ensuring that accurate dynamical behaviour is maintained [23]. Hence, once a distribution of moving charged particles has been introduced into this grid the EM fields can be computed by solving Maxwell's equations in discretized time, which in turn govern the subsequent motion on the particles. However, the fact that the discrete space of fields is disjoint from the continuous field of particles means that we need an approach to translate between them. We outline the general method to do this in figure 2.1, which involves an iterative loop of so-called particle push and field solver algorithms. We start by considering a known spacial distribution of particles and their associated velocities,  $(\mathbf{r}_n, \mathbf{v}_n)$ , at a time  $t_n$ . In order to compute the induced EM fields at discrete grid points the charged macroparticles are weighted onto several of the nearest grid points, thus resulting in each grid point having an associated charged distribution and current,  $(\rho_n, \mathbf{J}_n)$ . The corresponding EM fields, which we label by  $n + 1$  since these will act to move our particles, are found through

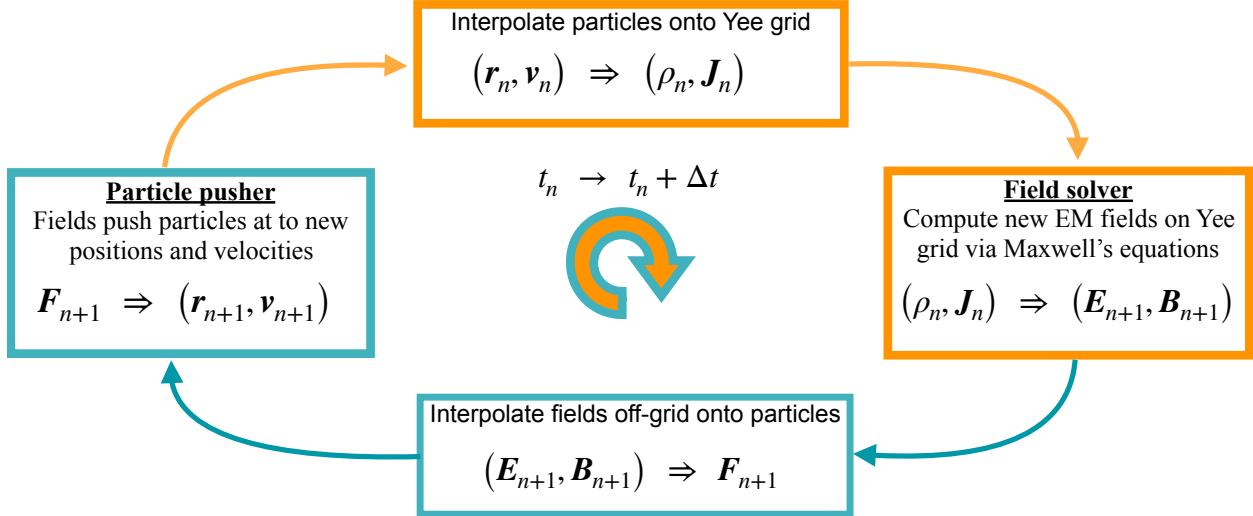


**Figure 2.1:** Flowchart showing the general operations conducted during one time iteration of the Particle-In-Cell simulation method. The colours indicate whether the EM fields and particle distributions are calculated at points on the discretized Yee grid (orange) or in the continuous space of particles (blue). The field update and particle push algorithms

Maxwell's equation via a *field solver* algorithm. This is necessitated by the fact that the EM fields at  $n+1$ ,  $(\mathbf{E}_{n+1}, \mathbf{B}_{n+1})$ , are not only sourced by  $\rho_n$  and  $\mathbf{J}_n$  but also by the variation of the fields,  $\Delta\mathbf{B}$  and  $\Delta\mathbf{E}$ , between  $n$  and  $n+1$  through Ampere's and Faraday's laws. Hence the fields can not be computed at the same time since, for instance,  $\mathbf{B}_{n+1}$  is in part induced by  $\Delta\mathbf{E} = \mathbf{E}_{n+1} - \mathbf{E}_n$ , where  $\mathbf{E}_{n+1}$  is in turn induced by  $\Delta\mathbf{B} = \mathbf{B}_{n+1} - \mathbf{B}_n$ . This issue is addressed by the *leapfrog* method, whereby particle positions and velocities are calculate at alternating half-way intermediate steps  $n + 1/2$ , but out of step by  $\Delta t/2$ . This means that we compute  $\mathbf{r}_n$  and  $\mathbf{v}_{n-1/2}$  simultaneously, followed by  $\mathbf{r}_{n+1}$  and  $\mathbf{v}_{n+1/2}$ . Although not immediately obvious, this allows us to calculate the EM fields in the following chain:  $(\mathbf{E}_n, \mathbf{B}_n) \rightarrow (\mathbf{E}_n, \mathbf{B}_{n+1/2}) \rightarrow (\mathbf{E}_{n+1}, \mathbf{B}_{n+1/2}) \rightarrow (\mathbf{E}_{n+1}, \mathbf{B}_{n+1})$ . It can further be shown that the truncation error per iteration scales as the square of the distance successive grid points [23], and is thus a second-order numerical simulation scheme. Once these fields are known the first step of the loop is effectively done in reverse by weighting the fields off the grid and back onto each individual macroparticle. Then using a similar leapfrog method in a *particle pusher* algorithm the Lorentz force law is used to push the particles to their new positions and velocities, thus completing the iteration step.

### 2.3 EPOCH

The Extensible PIC Open Collaboration project (EPOCH) is an advance relativistic electromagnetic PIC code developed at the University of Warwick [24]. EPOCH is now maintained and developed through the Collaborative Computational Project in Plasma Physics (CCP-Plasma), from which access to the code is granted to non-profit research laboratories and Universities [25]. The underlying code is written in Fortran and allows for simulations to be run on multiple parallel processors via MPI; this enables time-consuming simulations to be run on remote computing clusters. The core PIC code in EPOCH is based upon the field solver and particle push algorithms of the Plasma Simulation Code (PSC) written by H. Ruhl [26]. This follows closely the standard PIC

scehme outline in section 2.2. The main difference being the use of a more precise leapfrog method and the inclusion of additional functionality to allow for more advanced features such as collisions, ionisation and quantum electrodynamic radiation to be simulated. Furthermore, EPOCH is highly user-friendly; setting up simulations simply requires users to specify the parameters and initial conditions of the simulations without the need to interact with the underlying PIC code. Likewise, analysing and visualising data from a simulations is made easier through file-compatibility with Python, Matlab, IDL and VisIt.

### 2.3.1 Input deck

Once EPOCH has been downloaded and compiled the *input deck* is essentially EPOCH’s user interface. This is a text file in which users specify the details of a simulation to be passed onto EPOCH’s core PIC algorithm. It is composed of blocks which each specify different features of the simulations. The full details of all available blocks can be found in the EPOCH user manual [24]. The control, species and laser blocks are of particular importance to this project and will be covered briefly. In the *control block* the grid resolution, iteration time-steps and further details of the PIC scheme are specified. When defining the resolution of the grid one has to make sure that the grid is sufficiently fine such that the smallest features of our physical system are resolved. This is to ensure that the simulation accurately models the physical system it is meant to represent, to the extent that missing small-scale phenomena might alter the large scale outcome of the simulation. For instance, for laser-plasma interactions the wavelength of the laser ( $\sim 500$  nm) needs to be resolved by the grid spacing to ensure that the induced electron-oscillations are accurately modelled. A finer grid however requires more macroparticles to fully populate the grid, which inevitably extends the computational time. The grid is populated through *species block* where each species of particle, such as plasma electrons, plasma ions and electron beam driver, has a separate block. In these blocks, the number of macroparticels is specified together with the spatial and kinetic distributions of the particles. This allows us to, for instance, define a 1 GeV spherical electron bunch propagating through plasma with uniform or varying density. The introduction of a laser in the simulation is handled by the *laser block*, where parameters such as the laser intensity, pulse length and spot-size are defined. This differs from the species block in that the laser has to be attached to one edge of the simulation window and fired at  $t = 0$ , whereas the electron bunch can be initialised at any position at  $t = 0$ .

This posses two immediate issues for simulating the hybrid scheme: we require the laser to appear in front of the electron bunch, see figure 1.2(iv), while the current approach seems to at best allow us to initialise both the laser and bunch on top of each other at the beginning of the simulation window; we require the laser to fire after the bunch deceleration has saturated, see figure 1.2(iii), which is significantly after  $t = 0$ . The former of these issues was resolved by features in the input deck alone. Specially, it was found that the bunch could be initialised and held stationary for a given amount of time, such that a stationary bunch could be initialised ahead of the laser and subsequently released once the laser had propagated through and past then bunch. This approach however appeared to still affect the bunch, to the extent that high enough intensity lasers would pass through and disintegrate the stationary bunch. A work-around was found by setting the intensity of the laser to zero until it had passed the bunch, at which point the intensity was increased linearly to its maximum value. Although this solves both of the issues above, since the intensity could be kept zero until the bunch saturates, there are good reasons to seek a more efficient approach. The primary one being the computational cost of running these simulations. Indeed, even though we have been granted access to 24 Intel cores on the High-Performance Computing (HPC) cluster at the University of Manchester [27], many of the simulations we need to perform still require a few days up to to several weeks to finish. This would make the process of optimizing any parameters in the more intricate active beam dump very time-consuming, since the passive beam

dump would have to be simulated again following each minor change to the laser parameters for instance. It is therefore advantageous to divide up the simulation into separate passive and active beam dump simulations, where the latter then requires us to initialise a pre-saturated electron bunch together with a laser pulse. Crucially, however, the distributions functions in the input deck can only be defined analytically. Since previous studies [19, 21, 20] have shown that both the spatial and kinetic distributions of the electron driver after passing through a passive beam dump are highly non-analytical it is imperative that this issue be addressed if the hybrid beam dump is to be accurately simulated.

### 2.3.2 Non-analytical bunch initialisation

The hybrid scheme approach that the endeavour to investigate in this project relies on us being able to simulate a laser pulse propagating in front of a pre-saturated bunch. This was achieved by first exporting the data of the saturated bunch from a a passive beam dump simulation. The Self-Describing-File (SDF) data format used by EPOCH, however, is not suitable for easy access and retrieval of particular sets of data. A work-around was found by using the data-visualisation software VisIt [28] to read the files and export only the data related to the macroparticles of the electron bunch into a text file. In order to import this into a new simulation it was necessary to over-ride the electron bunch parameters in the input deck. Fortunately, EPOCH provides a file, `icmodule.f90`, which allows users to assigning custom values to each of the macroparticles that have been initialised in in the input deck. Hence, by initialising a standard spherical electron bunch in the input deck with the exact number of macroparticles that we exported from the passive simulation and reading in the exported data in the `icmodule.f90` file, we were able to loop over these particles and assign each one with a new charge, mass, position and velocity corresponding to a macroparticle in the exported data file. Consequently, the saturated bunch is completely replicated in this new simulation.

# 3

## Theoretical foundations

### 3.1 Introduction

Real accelerators operate at a range of beam parameters tailored to specific research purposes. In order to avoid having to set up week-long simulations for each minor change of parameters it is crucial to understand the theory underlying these plasma wakefield phenomena and to investigate to what extent the theoretical predictions match the simulations. Hence, in this chapter, the linear fluid model of plasma wakefield acceleration is introduced and the equations governing the plasma response to an electron beam driver are derived. We also briefly discuss the non-linear, so-called "blowout", regime which can not be treated perturbatively and is characterised by the expulsion of plasma electrons in a volume behind the bunch. The response to a laser being driven through the plasma, the so-called ponderomotive force response, shares many similar features to the theory presented in this chapter but presents other issues such as dissipation and de-phasing in the plasma which will need to be addressed in the context of the active beam dump. For this reason the theory of laser-plasma interactions will be covered in a subsequent report.

### 3.2 Linear fluid model

In this section, we derive the response of a plasma to an electron bunch by considering the plasma electrons as a fluid. We shall make the assumptions: (i) the initial plasma is uniform and electrically neutral everywhere; (ii) the plasma ions are stationary; (iii) the electron bunch is ultra-relativistic,  $v/c \approx 1$ , such that the density distribution of the bunch does not evolve significantly as it interacts with the plasma; (iv) the bunch density is much less than the plasma electron density,  $n_b \ll n_p$ . A beam propagating through a plasma satisfying these conditions is said to be in the *linear regime*. The dynamics of the plasma electrons is governed by the continuity equation

$$\frac{\partial n_p}{\partial t} = -\nabla \cdot (n_p \mathbf{v}_p) , \quad (3.1)$$

where  $n_p$  and  $\mathbf{v}_p$  are the plasma electron density density and fluid velocity. This simply ensures charge conservation by imposing that the plasma electron density change in a given volume is due to plasma electrons flowing in or out. The evolution of the electromagnetic fields in the plasma are governed by Maxwell's equations:

$$\nabla \cdot \mathbf{E} = 4\pi\rho , \quad (3.2)$$

$$\nabla \cdot \mathbf{B} = 0 , \quad (3.3)$$

$$\nabla \times \mathbf{E} = -\frac{1}{c} \frac{\partial \mathbf{B}}{\partial t} , \quad (3.4)$$

$$\nabla \times \mathbf{B} = \frac{4\pi}{c} \mathbf{J} + \frac{1}{c} \frac{\partial \mathbf{B}}{\partial t} , \quad (3.5)$$

where, as is convention in plasma physics, we work in CGS units. These fields in term determine the response of the plasma fluid through the Lorentz force law:

$$m_e \frac{\partial n_p \mathbf{v}_p}{\partial t} = en_p \left( \mathbf{E} + \frac{\mathbf{v}_p \times \mathbf{B}}{c} \right) . \quad (3.6)$$

We now make use of assumption (iv), which allows us to treat the plasma response to a particle beam perturbatively by defining the plasma-electron density  $n_p = n_0 + n_1$ , where  $n_0$  is the unperturbed uniform electron density and  $n_1 \ll n_0$ . This perturbation also requires that the change in fluid velocity upon impact with the bunch is small, such that  $v_p \ll c$ . Substituting this is into the continuity equation and neglecting terms  $\mathcal{O}(n_1/n_0)$  then yields

$$\frac{\partial^2 n_1}{\partial t^2} = -n_0 \frac{\partial(\nabla \cdot \mathbf{v}_p)}{\partial t} . \quad (3.7)$$

Similarly, substitution into the Lorentz force law simply leaves the electric force:

$$m_e \frac{\partial \mathbf{v}_p}{\partial t} = e\mathbf{E} , \quad (3.8)$$

which, using Gauss's law, gives

$$\frac{\partial(\nabla \cdot \mathbf{v}_p)}{\partial t} = \frac{e^2}{m_e} 4\pi(n_1 + n_b) \quad (3.9)$$

where we have introduced  $n_b$  as the density of the electron bunch. Equations (3.7) and (3.9) hence give

$$\frac{\partial^2 n_1}{\partial t^2} + \omega_p^2 n_1 = -\omega_p^2 n_b \quad (3.10)$$

where

$$\omega_p = \sqrt{\frac{4\pi e^2 n_0}{m_e}} \quad (3.11)$$

is the plasma frequency which determines the magnitude of the plasma-density perturbation. This justifies the stationary-ion assumption (ii) stated above, since for all plasmas the mass of the ions  $m_{\text{ion}} \gg m_e$  the ion-density perturbations will be negligible in comparison to the electron density. Hence the plasma-density perturbation is described by a second-order differential equation with the bunch acting as a source term. We proceed to solve this for a radially symmetric beam by evaluating equation (3.10) in a reference frame co-moving with the electron bunch [29] by defining  $\xi = z - ct$  as the position along the bunch as it travels in the  $z$ -direction. This yields that the co-moving density perturbations behind with the bunch satisfy

$$-\frac{1}{k_p^2} \left( \frac{\partial^2}{\partial \xi^2} + k_p^2 \right) n_1(r, \xi) = n_b(r, \xi) \quad (3.12)$$

where  $k_p = \omega_p/c$  is the wavenumber. We evaluate this by finding the Green's function  $G(\xi, \xi')$ , which by definition obeys

$$-\frac{1}{k_p^2} \left( \frac{\partial^2}{\partial \xi^2} + k_p^2 \right) G(\xi, \xi') = \delta(\xi - \xi') \quad (3.13)$$

where causality demands that  $G(\xi < 0, \xi') = 0$  such that

$$G(\xi, \xi') = \Theta(\xi - \xi') (A(\xi') \sin(k_p \xi) + B(\xi') \cos(k_p \xi)) \quad (3.14)$$

where  $\Theta(r)$  is the Heavieside step function and the constant  $A(\xi') = -k_p \cos(k_p \xi')$  and  $B(\xi') = k_p \sin(k_p \xi')$  are determined by requiring continuity at  $\xi = \xi'$ . The resulting plasma perturbation is therefore

$$n_1(r, \xi) = k_p \int_{-\infty}^{\xi} \sin(k_p(\xi - \xi')) n_b(r, \xi') d\xi' \quad (3.15)$$

where we have used the trigonometric identity for  $\sin(k_p(\xi - \xi'))$ . Hence the electron bunch induces oscillatory density perturbations in the plasma with a wavelength given by  $\lambda_p = 2\pi/k_p$ . In addition, the magnitude of these perturbation scales linearly with  $n_b$ , the density of the beam driver, and as  $n_0^{1/2}$ , the square root of the unperturbed plasma density through equation (3.11). These perturbations set up electromagnetic fields in the plasma behind the beam driver. An understanding of the electromagnetic fields that these perturbations induce is crucial to design a functioning plasma wakefield experiment.

### 3.2.1 Longitudinal accelerating field

The electric field parallel to the propagation of the beam driver, the so-called longitudinal plasma wakefield, drives particles to either accelerate or decelerate and consequently determines the efficiency of our plasma beam dump. Hence, in this section we derive an expression for this field in the linear regime considered above. From Maxwell's equations (3.2-3.5) it is straightforward to show that the electric field in the plasma obeys a wave equation:

$$\nabla^2 \mathbf{E} - \frac{1}{c^2} \frac{\partial^2 \mathbf{E}}{\partial t^2} = \frac{4\pi}{c^2} \frac{\partial \mathbf{J}}{\partial t} + 4\pi \nabla \rho , \quad (3.16)$$

where the change in the current  $\mathbf{J} = \mathbf{J}_b + \mathbf{J}_p$  and variations in the charge density  $\rho = \rho_b + \rho_p$  act as source terms. Furthermore, we have from equation (3.8) that

$$\frac{\partial \mathbf{J}_p}{\partial t} = \frac{e^2 n}{m_e} \mathbf{E} . \quad (3.17)$$

Substituting this into equation (3.16), together with the an ultra-relativistic beam current  $\mathbf{J}_b = c\rho_b \hat{\mathbf{z}}$ , gives that the longitudinal wakefield  $E_z$  satisfies

$$\left( \nabla^2 - \frac{1}{c^2} \frac{\partial^2}{\partial t^2} - k_p^2 \right) E_z = \frac{4\pi}{c} \frac{\partial \rho_b}{\partial t} + 4\pi \frac{\partial}{\partial z} (\rho_b + \rho_p) , \quad (3.18)$$

where  $k_p = \omega_p/c$  is the plasma wave number. To solve this we assume that  $E_z$  is radially symmetric and write the Laplace operator in cylindrical polar coordinates,  $\nabla^2 = \nabla_\perp^2 + \frac{\partial^2}{\partial z^2}$ , where the transverse component

$$\nabla_\perp^2 = \frac{1}{r} \frac{\partial}{\partial r} r \frac{\partial}{\partial r} + \frac{1}{r^2} \frac{\partial^2}{\partial \phi^2} . \quad (3.19)$$

Furthermore, the derivation is simplified by working in Fourier transform space, where

$$E_z(\xi) = \frac{1}{2\pi} \int_{-\infty}^{\infty} \tilde{E}_z(k) e^{ik\xi} dk , \quad (3.20)$$

and similarly for  $\rho_b$  and  $\rho_p$ . Equation (3.18) then simplifies to

$$\left( \nabla_\perp^2 - k_p^2 \right) \tilde{E}_z(\xi) = 4\pi i k \tilde{\rho}_p , \quad (3.21)$$

We note that in this form the two contributions from the beam,  $\mathbf{J}_b$  and  $\rho_b$ , have cancelled each other out. This is because the beam velocity was set to  $\beta = 1$ , such that the electric field of the

beam itself is purely in the radial direction [30]. The effect of the beam is however represented in the plasma modulations  $\tilde{\rho}_p$  through equation (3.15). Given that experimentally the beam density is often known, and the plasma perturbations can only be inferred from data, it is convenient to write this relationship in a compact form by taking the Fourier transform of equation (3.10), such that

$$\left( \frac{\partial^2}{\partial r^2} + \frac{1}{r} \frac{\partial}{\partial r} - k_p^2 \right) \tilde{E}_z = 4\pi i k_p^2 \frac{k}{k^2 - k_p^2} \tilde{\rho}_b \quad (3.22)$$

which we define in a compact form as  $\mathcal{L}\tilde{E}_z = \tilde{f}(r, k)$ . This is the Fourier transformed version of equation (3.18), which has the advantage of the source term  $\tilde{f}(r, k)$  being a function of the beam density alone. Hence by solving this PDE we can find  $E_z$  through an inverse Fourier transform. This is again done by finding its Green's function,  $G(\mathbf{r}, \mathbf{r}')$ , which in cylindrical coordinate satisfies

$$\mathcal{L}G(\mathbf{r}, \mathbf{r}') = \frac{1}{r} \delta(r - r') \delta(\phi - \phi') \delta(z - z') \quad (3.23)$$

where the delta function has been written in cylindrical polar coordinates. Since the PDE is radial we can write the Green's function as

$$G(\mathbf{r}, \mathbf{r}') = G_r(r, r') \delta(\phi - \phi') \delta(z - z') \quad (3.24)$$

which leads to

$$\mathcal{L}G_r(r, r') = \frac{1}{r} \delta(r - r') \quad (3.25)$$

where left-hand side is the modified Bessel function of order zero [31]. Consequently, the Green's function is formed by linear combinations of the modified Bessel functions of order zero, denoted by  $K_0$  and  $I_0$ :

$$G(r, r') = \begin{cases} A(r')(A_1 I_0(k_p r) + B_1 K_0(k_p r)) & , 0 < r < r' \\ B(r')(A_2 I_0(k_p r) + B_2 K_0(k_p r)) & , r' < r < \infty . \end{cases} \quad (3.26)$$

By requiring that the two parts of this expression each satisfy one of the boundary conditions, namely that the functions are finite at  $r = 0$  and tend to zero as  $r \rightarrow \infty$ , we have that  $B_1 = A_2 = 0$ . Continuity in  $G(r, r')$  at  $r = r'$  further gives that

$$G(r, r') = A_0 \begin{cases} I_0(k_p r) K_0(k_p r') & , 0 < r < r' \\ I_0(k_p r') K_0(k_p r) & , r' < r < \infty \end{cases} \quad (3.27)$$

where  $A_0$  is a constant of proportionality that we find by integrating equation (3.25) across the interval  $r \in [r' - \epsilon, r' + \epsilon]$ . This expression needs to be satisfied for all  $\epsilon$ , including the limit as  $\epsilon \rightarrow 0$ , such that

$$\lim_{\epsilon \rightarrow 0} \int_{r' - \epsilon}^{r' + \epsilon} \mathcal{L}G_r(r, r') dr = \lim_{\epsilon \rightarrow 0} \int_{r' - \epsilon}^{r' + \epsilon} \frac{1}{r} \delta(r - r') dr \quad (3.28)$$

which implies that  $A_0 = -1$  and that

$$G(r, r') = -I_0(k_p r) K_0(k_p r') \Theta(r' - r) - I_0(k_p r') K_0(k_p r) \Theta(r - r') . \quad (3.29)$$

We can thus find  $\tilde{E}_z$  from

$$\tilde{E}_z(r, k) = \int_0^\infty G(r, r') f(r', k) r' dr' \quad (3.30)$$

and then perform an inverse Fourier transform to find the co-moving longitudinal wakefield:

$$E_z(r, \xi) = -2ik_p^2 \int_{-\infty}^{\infty} \frac{ke^{ik\xi}}{k^2 - k_p^2} dk \int_0^\infty G(r, r') \tilde{\rho}_b(r') r' dr' \quad (3.31)$$

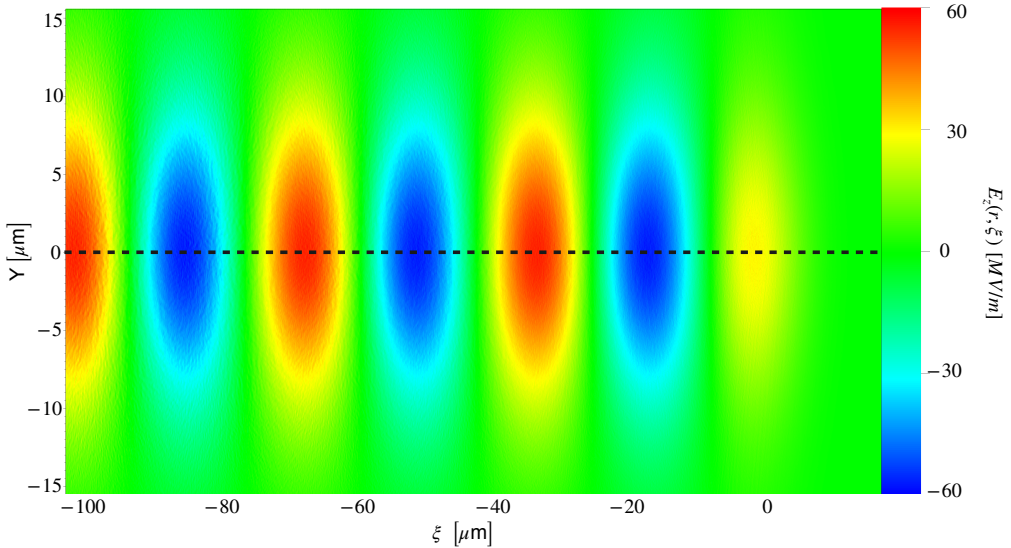


**Figure 3.1:** Two-dimensional simulation plot of the co-moving longitudinal electric field in the linear regime,  $n_p = 100n_b$ . The electron bunch (not shown) is centred on  $\xi = 0$  and moves to the right.

For a known beam distribution  $\rho_b(r, \xi)$  this expression can be used to compute the resulting longitudinal electric field. Of particular interest to us is the field induced by the propagation of an electron bunch that is Gaussian in both the transverse and longitudinal direction, a so-called bi-Gaussian bunch. To compute this we follow an approach by Dawson [32] and first evaluate the field due to a point-particle and then convolve it with our bi-Gaussian driver. We choose a radially symmetric point-particle distribution  $\rho_0(r, \xi)$  to match our Green's function:

$$\rho_0(r, \xi) = -\frac{e}{2\pi r} \delta(r - r') \delta(\xi) \quad (3.32)$$

Substituting the Fourier transform of this into equation (3.31) and performing a contour integrating in k-space yields

$$E_z(r, \xi) = 2ek_p^2 \cos(k_p \xi) G(r, r') \Theta(\xi), \quad (3.33)$$

where  $\Theta(\xi)$  ensures causality is preserved. This is the so called single-particle wake function [32]. The longitudinal electric field resulting from an arbitrary radially-symmetric source distribution  $n_b(r, \xi)$  is now given by convolving the source by the single-particle wake function:

$$E_z(r, \xi) = 2ek_p^2 \int_0^{2\pi} d\phi \int_{-\infty}^{\infty} \cos(k_p(\xi - \xi')) \Theta(\xi - \xi') d\xi' \int_0^{\infty} G(r, r') n_b(r', \xi') r' dr' \quad (3.34)$$

To compare with simulations and experiments we now choose to convert from CGS to SI units by having  $e^{\text{CGS}} \rightarrow e^{\text{SI}} / \sqrt{4\pi\epsilon_0}$ . The longitudinal wakefield in SI units (J/m) is thus

$$E_z(r, \xi) = \frac{ek_p^2}{\epsilon_0} \int_{-\infty}^{\xi} \cos(k_p(\xi - \xi')) d\xi' \int_0^{\infty} G(r, r') n_b(r', \xi') r' dr' \quad (3.35)$$

To test the validity of the linear fluid model as well as highlight some key features of the longitudinal wakefield we will calculate this field numerically for a 1 GeV bi-Gaussian bunch with a density of the form

$$n_b(r, \xi) = \frac{N_b}{(2\pi)^{3/2} \sigma_r^2 \sigma_\xi} e^{-\xi/(2\sigma_\xi^2) - r/(2\sigma_r^2)} \quad (3.36)$$

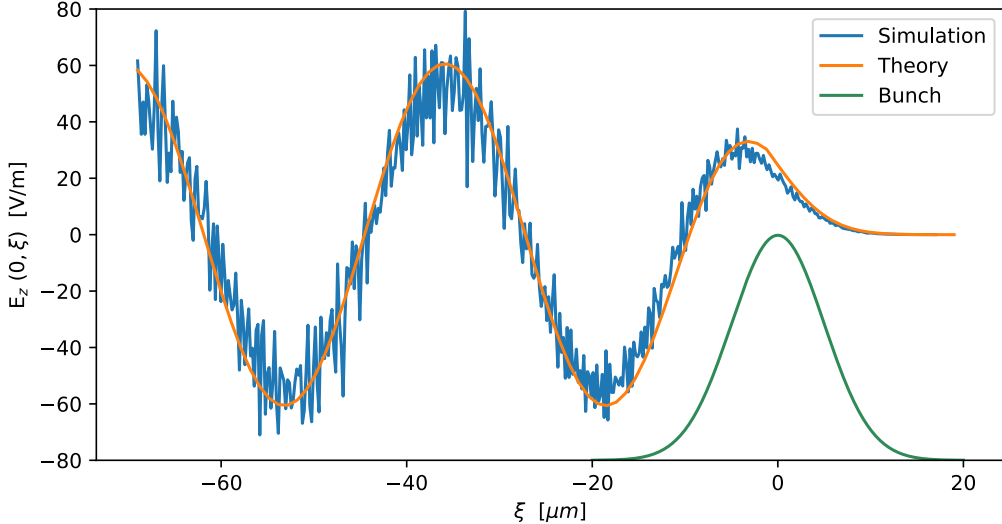


**Figure 3.2:** Plot comparing the longitudinal wakefield on axis,  $r = 0$ , for PIC simulation and linear fluid theory for  $n_p/n_b = 100$ . The simulation data corresponds to values along the dotted line in figure 3.1. The theory prediction is given by equation (3.35). The Gaussian bunch distribution in the longitudinal direction is also shown.

where  $N_b$  is the number of electrons in the bunch and  $\sigma_\xi$  and  $\sigma_r$  are the standard deviation of the bunch in the longitudinal and transverse direction. At this stage we will also compare these calculations to equivalent two-dimensional PIC simulations using EPOCH, as described in chapter 2. We choose a plasma density  $n_p = 100n_b$  to ensure that the electron beam is in the linear regime. We also set the bunch dimensions to  $\sigma_\xi = \sigma_r = 5 \mu\text{m}$  and  $N_b = 10^6$  to allow for later comparisons with the simulations presented in chapter 4. The beam dump that we have in mind will not necessarily have the beam in the linear regime, however the linear-regime simulations in this chapter will function as a benchmark for the validity of the linear model. The resulting two-dimensional co-moving longitudinal wakefield from this simulations is shown in figure (3.1), where the beam has propagated only  $200 \mu\text{m}$  to the right to minimize bunch distortions. Remembering that these fields are induced by electron density modulations this plot clearly shows the oscillatory density-perturbations described by equation (3.15). To allow for comparison with equation (3.35) we extract the data for the electric field at  $Y = 0$  and compare to calculations at  $r = |y| = 0$ , the result of which is shown in figure 3.2. We note that the theoretical calculations and the simulations are indeed in good agreement, with the linear model predicting both the amplitude and the wavelength of the induced plasma wakefield. We also note that the electric field is positive along the bunch, implying that there is a decelerating force on the electron bunch. We can also identify some of the features that previous studies have found. In particular, the energy chirp found by Wu et. al, figure 1.1, can be explained by the fact that both theory and simulation predict that the head of the bunch,  $\xi > 0$ , should experience a near-zero electric field. As a result, energy loss should only occur through scattering mechanisms, which are entirely negligible compared to the effect of this wakefield [19]. We may furthermore predict that this method can not fully deplete the energy of the beam on its own. For, assuming that the electric field maintains its form as the beam propagates, as soon as particles lose enough energy to fall behind the rest of the bunch, they will end up in a region of negative electric field,  $-25 < \xi < -15 \mu\text{m}$ , and subsequently get re-accelerated. One method for dealing with this was described in chapter 1, whereby Wu et al. [19] simulated the use of foils to prevent particles reaching the re-acceleration region. The other method, proposed by Hanahoe et al. [20] was to let the beam propagate through an increasing plasma density. Although this method has not been simulated so far, if the proposed experiments

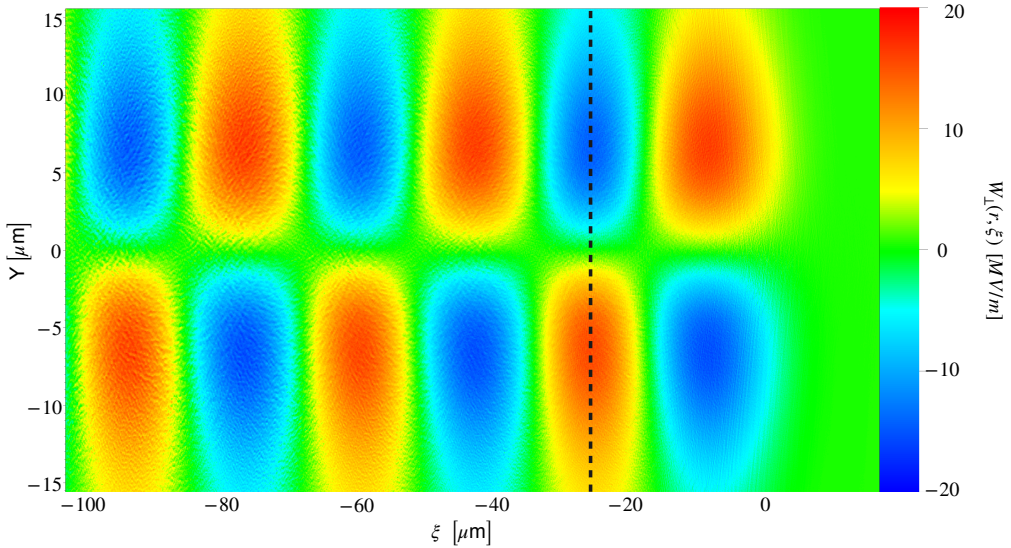


**Figure 3.3:** Two-dimensional simulation plot of the co-moving transverse wakefield in the linear regime,  $n_p = 100n_b$ , showing successive focusing and defocusing regions. The electron bunch (not shown) is centred on  $\xi = 0$  and moves to the right.

at FLASHForward at DESY in 2019 include the possibility to test this proposal this method will need to be explored further in the upcoming report. This method utilizes transverse wakefields, which we cover below for completeness.

### 3.2.2 Transverse field

Relative to the stationary plasma electrons an ultra-relativistic electron bunch will be fully Lorentz contracted in its direction of propagation, with a purely radial electric field. Consequently, the plasma electrons will be displaced radially, which not only act to set up the longitudinal wakefield we calculated above but also a radial restoring field,  $E_r$ . In addition, the electron bunch induce an azimuthal magnetic field,  $B_\theta$ , which further affect the plasma electrons. The resulting transverse wakefield,  $W_\perp = E_r - cB_\theta$ , will also affect the electron bunch itself. The wakefield experienced by an ultra-relativistic electron in the bunch is given by the *Panofsky-Wenzel theorem* [33], which says that the transverse wakefield at a position  $\xi < 0$  behind the bunch is related to the longitudinal wakefield  $W_\parallel$  via

$$\frac{\partial W_\perp}{\partial z} = \frac{\partial W_\parallel}{\partial r}, \quad (3.37)$$

where, in our case,  $W_\parallel = E_z$  such that

$$W_\perp(r, \xi) = \int \frac{\partial E_z(r, \xi)}{\partial r} dz. \quad (3.38)$$

The transverse force on a bi-Gaussian bunch can now be found by applying this expression to the longitudinal single-particle wakefield (3.33) and then performing the same convolution as above [32, 34], which yields

$$W_\perp(r, \xi) = \frac{ek_p}{\epsilon_0} \int_{-\infty}^{\xi} \sin(k_p(\xi - \xi')) d\xi' \int_0^{\infty} \frac{\partial G(r, r')}{\partial r} \frac{n_b(r', \xi')}{\partial r'} r' dr' \quad (3.39)$$

For consistency we also extract  $E_r$  and  $B_\theta$  from the same simulation as above and plot  $W_\perp$  in figure 3.3. From this we note that the radial field exhibits the same longitudinal oscillatory behaviour that we have seen before, with equation (3.39) saying that the phase of the transverse and

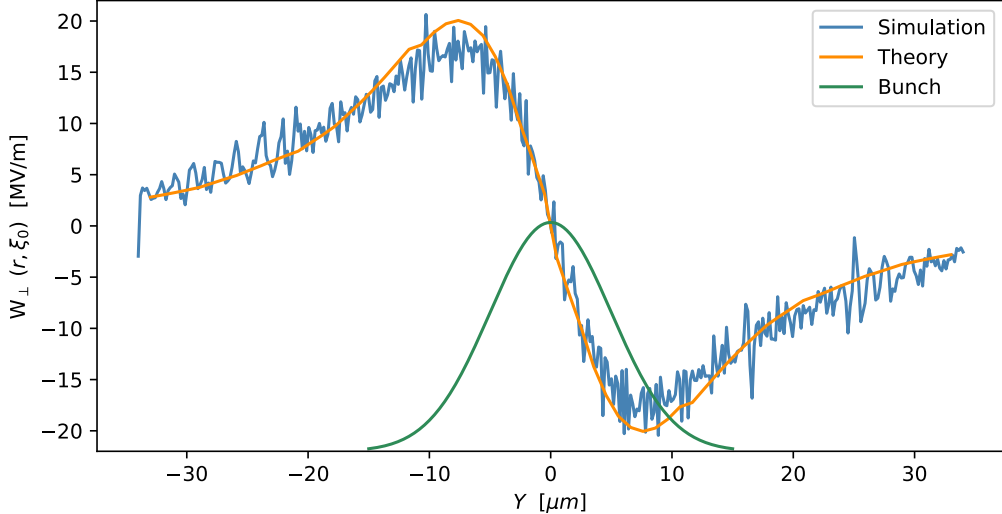


**Figure 3.4:** Plot comparing the co-moving transverse wakefield at  $\xi = -25 \mu\text{m}$ , for PIC simulation and linear fluid theory for  $n_p/n_b = 100$ . The simulation data corresponds to values along the dotted line in figure 3.3, the theory prediction is given by equation (3.39) and the Gaussian bunch distribution in the transverse direction is also shown.

longitudinal fields differ by  $\pi/2$ . In contrast to before, however, we also have radial oscillations. This is of particular importance to plasma wakefield acceleration experiments, since it implies that there will be a region which is simultaneously accelerating and focusing, enabling high acceleration of narrow beams [6]. Hanahoe et al. [20] was able to use a similar approach to show that by employing a varying density one could find that re-acceleration of particles that had fallen behind the bunch occurred in a de-focusing region. Thereby forcing the particles outwards, where they were subsequently decelerated through ordinary scattering. In fact, the dotted line in figure 3.3 shows such a de-focusing region, since  $W_\perp < 0$  act to drive electrons to increasing  $Y$  values and vice versa. Figure 3.4 shows that this field is again in good agreement with the linear fluid theory predictions of equation (3.39).

### 3.2.3 Plasma deceleration

Electrons in the bunch that are in a decelerating region will lose energy; this is the general idea behind the plasma beam dump. Since we can calculate the electric field at any position  $(\xi, r)$  along the bunch we can estimate the energy loss by calculating the work carried out by the longitudinal electric field. This is the approach taken by Bonatto et al. [35] to estimate the distance required to dump various beams in their passive or active plasma beam-dump scenarios. Assuming that there occurs no modulation of the particle bunch as it propagates through the plasma, the energy of one particle in the beam at position  $(r, \xi)$  after travelling a distance  $s$  is given by:

$$U_e(r, \xi, s) = U_e(r, \xi, 0) - seE_z(r, \xi) , \quad (3.40)$$

from which multiplication by the beam number density  $n_b(r, \xi)$  and integration over the volume of the bunch gives the total energy of all particles in the bunch as a function of propagation distance:

$$U(s) = \int U_0 - se \int E_z(r, \xi) n_b(r, \xi) r dr d\xi d\phi \quad (3.41)$$

where  $E_z$  and  $n_b$  are found from equations (3.35) and (3.36). A program to compute this numerically has not yet been implemented, but we endeavour to do so in the latter part of this project to allow for comparisons between the linear theory and simulations.

# 4

## Simulation tests

### 4.1 Bunch parameters

The intimal phase of this project involves simulating beam dumping of the proposed electron beam of the EuPRAXIA project. This is a European Union Horizon 2020 research project with the aim of developing a conceptual design report for a high-quality compact 5 GeV electron plasma wakefield accelerator for application in research and medicine [36]. Currently the studies are concerned with achieving high-quality 1 GeV electron beams. As the simulations and experiments yield successful results at this energy, higher energies will be explored until the 5 GeV goal is reached. Current target values for the electron bunch parameters are given in table 4.1, where case 1 and 2 represents laser-driven and beam-driven driven accelerators respectively [36]. In addition, parameters are shown for the simulated 1 GeV electron beam that we aim to dump. These differ in two key aspects to the other EuPRAXIA cases. Firstly, the energy spread and emittance of the bunch have been lowered. This lowers the computational cost of running these simulations, by effectively decreasing the relative motion of the particles in the bunch, while still maintaining a realistic beam quality [37]. Secondly, the size of the bi-Gaussian bunch has been increased significantly because of the fact that the current parameters would lead to bunch densities in excess of  $10^{20}\text{cm}^{-3}$ , making neither linear nor quasilinear regimes accessible with conventional plasma sources. Plasma densities  $\sim 10^{20}\text{cm}^{-3}$  are achievable using supersonic gas jets [38] – where a high-density gas jet is ionised into a plasma using a laser – however the novelty and impracticality of this technique lead us to instead lower the bunch density. Expansion of the bunch in the radial direction could be achieved by simply letting the bunch propagate freely in a vacuum, at which point the bunch would expand due to its space-charge force, while longitudinal stretching is achievable using conventional so-called magnetic chicanes [39]. We choose here to expand the dimensions of the bunch to  $\sigma_\xi = \sigma_r = 5\text{\mu m}$ . This is chosen in part to give a more workable bunch density of  $n_b = 10^{17}\text{cm}^{-3}$ , as well as to allow for comparisons with existing free-electron laser and plasma wakefield experiments, which tend to have bunch dimensions in the single to tens of micrometer range.

EuPRAXIA bunch parameters			
Parameter	Case 1	Case 2	Simulations
Energy	5 GeV	3 GeV	1 GeV
Charge	100 pC	30pC	30pC
Bunch length $\sigma_\xi$ (RMS)	1.5 $\mu\text{m}$	0.9 $\mu\text{m}$	5.0 $\mu\text{m}$
Bunch width $\sigma_r$ (RMS)	0.3 $\mu\text{m}$	0.3 $\mu\text{m}$	5.0 $\mu\text{m}$
Energy spread (RMS)	5%	5%	1%
Transverse divergence (RMS)	0.32 mrad	0.41 mrad	10 $\mu\text{rad}$

**Table 4.1:** Parameters for the accelerated electron bunch in the EuPRAXIA project for laser-driven (case 1) and beam-driven (case 2) plasma wakefield accelerators. Parameters for the simulated beam used in our hybrid scheme study are also shown.

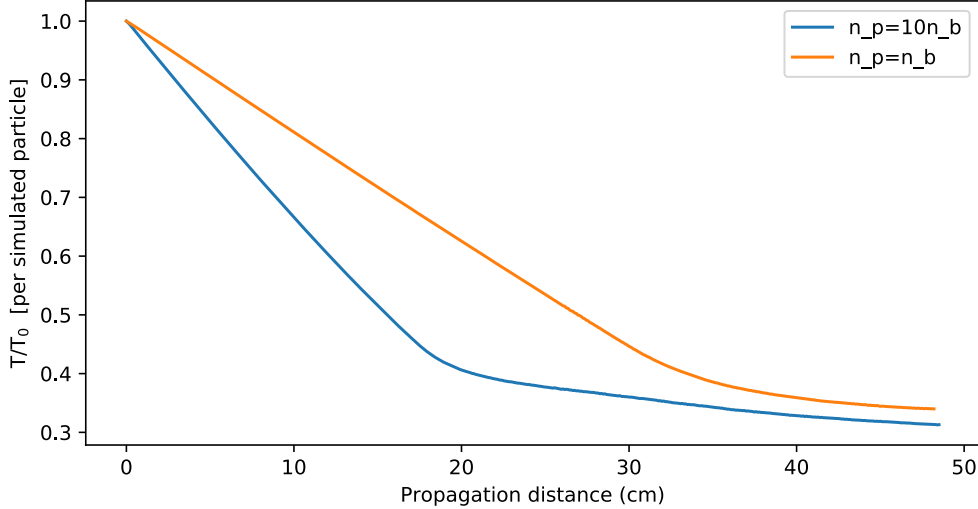


Figure 4.1: •

## 4.2 Linear and quasilinear regimes

In this section we present results for simulations in the linear regime, where the plasma density  $n_p = 10n_b$ , and the so-called quasilinear regime, where  $n_p = n_b$ , for the bunch parameters given in table 4.1. The remaining fraction of the initial bunch energy, per particle, for this bunches is plotted in figure 4.1 as a function of the propagation distance through these two plasmas. We note that, as found by Wu et al. [19] the energy loss in both regimes decreases linearly until the energy saturates at around 30-40%. We further note that saturation is reached faster in the linear regime than in the quasilinear regime, which is simply due to the fact that the magnitude of the decelerating field predicted by equation 3.35 scales linearly with plasma density. It is instructive to look at both these regimes in further detail.

Figure 4.4 shows the longitudinal wakefield, the energy distribution and spatial distribution of the linear bunch at two positions. Specifically, at (a) 20cm, when the energy is starting to level off, and (b) 48cm, when the energy is fully saturated. At both positions there is a clear energy chirp at the head of the bunch which experiences a near-zero electric field. In figure (a) we also see clear signs of re-acceleration, where particles in the bunch has been decelerated, fallen behind, and gotten caught in two regions: where the sign of the electric field changes and the minimum of the electric field. In figure (b) the bunch has split into four distinct parts and we note a low-energy tail around  $\xi = -20\mu\text{m}$ . This could potentially be removed using absorbing material as we described in figure 1.2. The large central re-acceleration peak however is not suitable for the hybrid scheme we have in mind, since we seek a single energy peak to dump with a laser. A solution is to increase the wavelength of the longitudinal wakefield by lowering the plasma density, which takes us into the quasilinear regime.

The linear simulations were conducted with a grid size of  $1\mu\text{m} \times 1\mu\text{m}$ , each grid point populated with 6 macroparticles and the simulation ran on 24 cores for 72 hours. This proved sufficient to resolve the bunch and the plasma wavelength with several grid points to ensure that no small-scale phenomena were modelled. When the same resolution was used for the quasilinear simulations we encountered large transverse instabilities. Figure 4.3 shows the emergence of the instabilities and the resulting disintegration of the bunch. This beam dispersion appeared at first to be a promising approach for rapid beam deceleration. Indeed, several beam instabilities are known to occur in beam-driven plasma wakefield acceleration. The *hosing instability* [40] exhibits similar formation as in figure 4.3 at 3 and 6 cm and appeared a good candidate. However, in discuss with colleagues

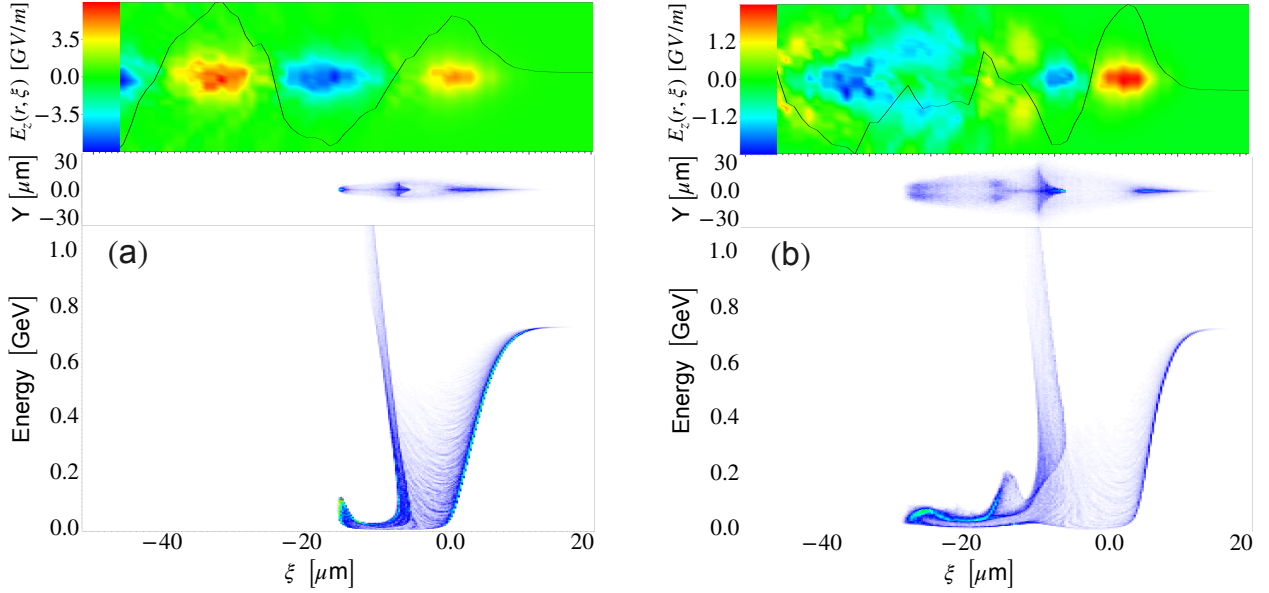


**Figure 4.2:** •

it was found that this is likely to be a numerical artefact in the PIC code known as the *numerical Cherenkov instability*. This is in fact a prevalent numerical issue in all relativistic PIC codes [41]. It arises in the PIC loop, described in figure 2.1, as a result of the different treatment of particles and fields [42]. This introduces deviations from the correct velocities of the particles in the beam, which leads to unphysical emission of Cherenkov radiation [41]. It appears that these emissions introduce microscopic instabilities which are amplified by the collective motion of the electrons. Although several grid and algorithm modifications exists in many PIC codes to reduce the effect of these numerical artefact, there is no secure way to avoid them other than to increase the grid and macroparticle resolution. A grid size of  $0.1\mu\text{m} \times 0.1\mu\text{m}$ , with each grid point populated with 10 macroparticles proved succesful in mitigating these effects. The simulation needed to run on 24 cores for 14 days before completion. The energy loss is given in figure 4.1, and the corresponding fields and distributions are given in figure ??.

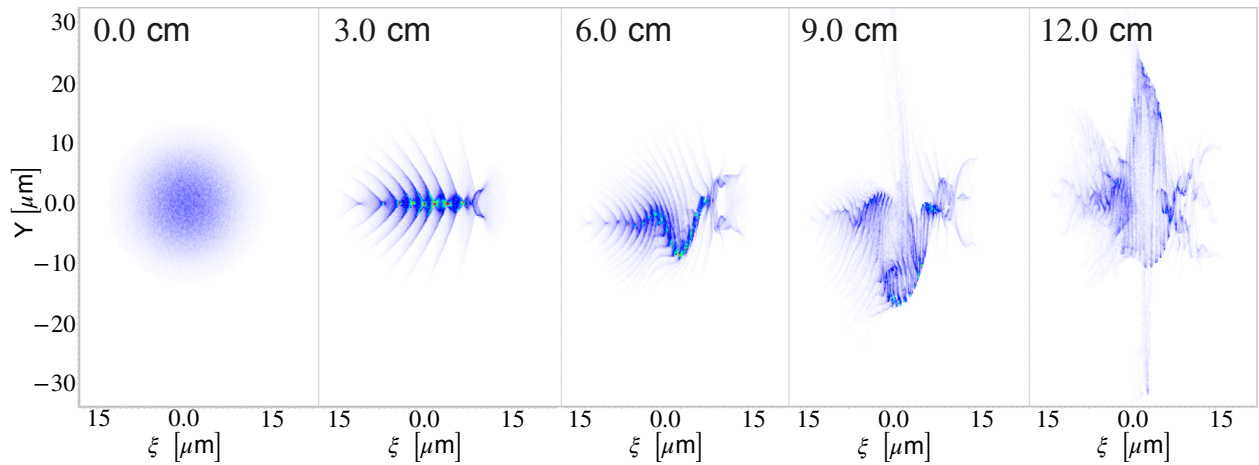


**Figure 4.3:** abc

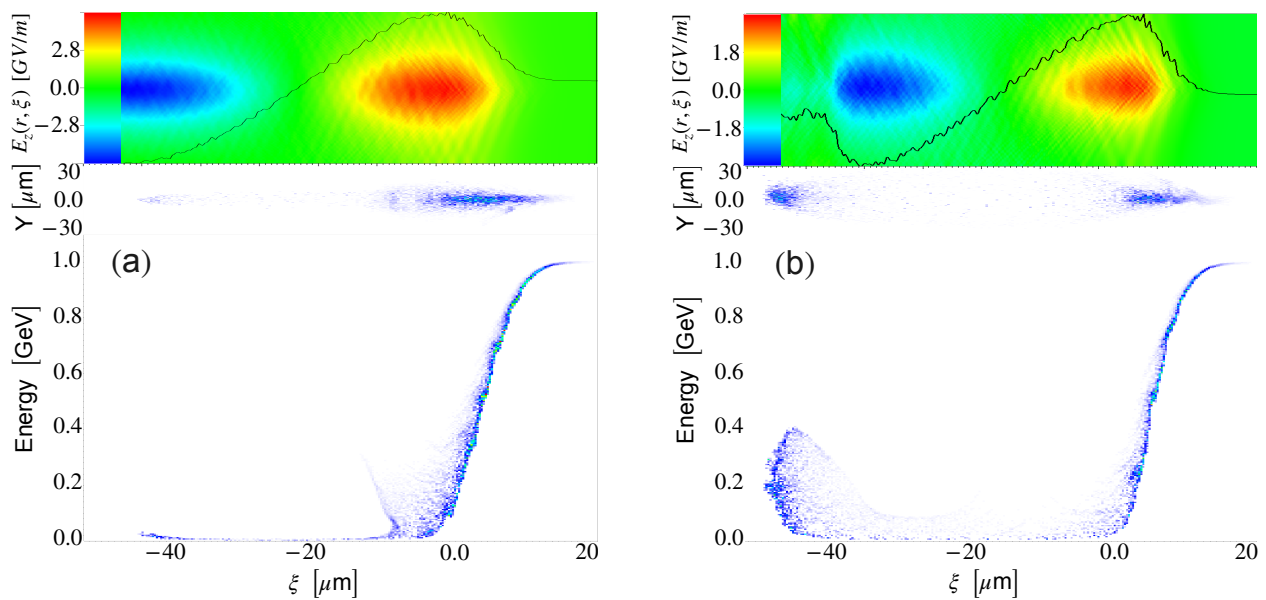


**Figure 4.4:** •

# 5

## Current work and concluding remarks

Having constructed the necessary computational framework for simulating the hybrid beam dump scheme we can now investigate the feasibility of this scheme and proceed to work out the details of the bunch-laser interaction. This will include investigating and optimizing the distance at which the laser is introduced, the spatial separation between the bunch and the the laser, the intensity and pulse length of the laser and effects caused by the difference in phase velocity between the bunch and the laser.

Once the details of the hybrid scheme has been investigated and a desirable approach has been determined we should proceed by high resolution simulations to verify that that the scheme works. As we have seen in section XXX the effect of insufficiently high simulation resolution can yield wildly different outcomes, as small effects can become amplified or neglected, in comparison to higher resolution runs. Consequently, in order to obtain reliable results from our simulations it is crucial to investigate the parameters that determine the resolution of the simulation. These include:

- The number of grid points: where a finer grid will increase the spatial resolution by having the macro-particles in adjacent grid cells be closer together, thus allowing the distribution of the plasma and bunch electrons to be more accurately modelled. This however comes at the cost of longer computational time.
- The number of macro particles in each grid cell: this has the same effect as using a finer grid by allowing the contents of grid cells to more accurately describe the distribution of micro-particles in those cells, since if only one macroparticle was used in a cell with electrons of varying energy and momentum that macroparticle would have to average these properties and thus remove the finer details of the plasma and bunch.
- The number of macro particles in the electron bunch: This number is crucial to accurately capture the small-scale effects on the bunch caused by the interaction with the plasma electrons.

How to establish these simulation parameters?

## 5. Current work and concluding remarks

---

We may divide the work on the hybrid scheme into three broad areas.

- Energy loss w.r.t bunch and plasma parameters
  - Eloss(bean width)
  - Eloss(length)
  - Eloss( $n_p/n_b$ ), where  $n_p = n_p$ (beam width, beam length)
- Simulation parameters
  - Grid settings and resolution to avoid transverse instabilities
  - Minimise numerical noise using laser ramp
  - Accuracy vs. Computational cost
- Laser driver
  - Optimise laser parameters
    - \* Time when introduced in simulation (at/before saturation)
    - \* Distance from bunch
    - \* Pulse length
    - \* Intensity, wavelength
    - \* Laser ramp
  - Further laser investigations
    - \* Multiple consecutive laser pulses

# 6

## Conclusion

Lorem ipsum dolor sit amet, consectetur adipisicing elit, sed do eiusmod tempor incididunt ut labore et dolore magna aliqua. Ut enim ad minim veniam, quis nostrud exercitation ullamco laboris nisi ut aliquip ex ea commodo consequat. Duis aute irure dolor in reprehenderit in voluptate velit esse cillum dolore eu fugiat nulla pariatur. Excepteur sint occaecat cupidatat non proident, sunt in culpa qui officia deserunt mollit anim id est laborum.

## 6. Conclusion

---

# Bibliography

- [1] The Technical Design Report (TDR) of the European XFEL.
- [2] David T. Attwood, Anne Sakdinawat, and Linda Geniesse. *X-rays and extreme ultraviolet radiation : principles and applications.*
- [3] Z Insepov, J Norem, A Bross, A Moretti, Z Qian, Y Torun, D Huang, R A Rimmer, S Mhalilingam, and S Veitzer. A model of rf breakdown arcs. Technical report, 2008.
- [4] Pisin Chen, Toshiki Tajima, and Yoshiyuki Takahashi. Plasma Wakefield Acceleration for Ultrahigh-Energy Cosmic Rays. *Physical Review Letters*, 89(16):14–17, 2002.
- [5] T Tajima and J M Dawson. Laser Electron Accelerator. Technical Report 4, 1979.
- [6] E. Esarey, C. B. Schroeder, and W. P. Leemans. Physics of laser-driven plasma-based electron accelerators. *Reviews of Modern Physics*, 81(3):1229–1285, 2009.
- [7] Donna Strickland and Gerard Mourou. Compression of amplified chirped optical pulses. Technical report, 1985.
- [8] C. E. Clayton, K. A. Marsh, A. Dyson, M. Everett, A. Lal, W. P. Leemans, R. Williams, and C. Joshi. Ultrahigh-gradient acceleration of injected electrons by laser-excited relativistic electron plasma waves. *Physical Review Letters*, 70(1):37–40, jan 1993.
- [9] W P Leemans, B Nagler, A J Gonsalves, K Nakamura, C G R Geddes, E Esarey, C B Schroeder, and S M Hooker. GeV electron beams from a centimetre-scale accelerator.
- [10] Xiaoming Wang, Rafal Zgadzaj, Neil Fazel, Zhengyan Li, S. A. Yi, Xi Zhang, Watson Henderson, Y.-Y. Chang, R. Korzekwa, H.-E. Tsai, C.-H. Pai, H. Quevedo, G. Dyer, E. Gaul, M. Martinez, A. C. Bernstein, T. Borger, M. Spinks, M. Donovan, V. Khudik, G. Shvets, T. Ditmire, and M. C. Downer. Quasi-monoenergetic laser-plasma acceleration of electrons to 2-GeV. *Nature Communications*, 4(1):1988, dec 2013.
- [11] W.-P. Leemans, A.-J. Gonsalves, H.-S. Mao, K. Nakamura, C. Benedetti, C.-B. Schroeder, Cs. Tóth, J. Daniels, D.-E. Mittelberger, S.-S. Bulanov, J.-L. Vay, C.-G.-R. Geddes, and E. Esarey. Multi-GeV Electron Beams from Capillary-Discharge-Guided Subpetawatt Laser Pulses in the Self-Trapping Regime. *Physical Review Letters*, 113(24):245002, dec 2014.
- [12] Zhirong Huang, Yuantao Ding, and Carl B. Schroeder. Compact X-ray Free-Electron Laser from a Laser-Plasma Accelerator Using a Transverse-Gradient Undulator. *Physical Review Letters*, 109(20):204801, nov 2012.
- [13] Preliminary Conceptual Design Report for the FACET-II Project at SLAC National Accelerator Laboratory. Technical report.
- [14] E. Adli, A. Ahuja, O. Apsimon, R. Apsimon, A. M. Bachmann, D. Barrientos, F. Batsch, J. Bauche, V. K. Berglyd Olsen, M. Bernardini, T. Bohl, C. Bracco, F. Braunmüller, G. Burt,

- B. Buttenschön, A. Caldwell, M. Cascella, J. Chappell, E. Chevallay, M. Chung, D. Cooke, H. Damerau, L. Deacon, L. H. Deubner, A. Dexter, S. Doeberl, J. Farmer, V. N. Fedosseev, R. Fiorito, R. A. Fonseca, F. Friebel, L. Garolfi, S. Gessner, I. Gorgisyan, A. A. Gorn, E. Granados, O. Grulke, E. Gschwendtner, J. Hansen, A. Helm, J. R. Henderson, M. Hüther, M. Ibison, L. Jensen, S. Jolly, F. Keeble, S. Y. Kim, F. Kraus, Y. Li, S. Liu, N. Lopes, K. V. Lotov, L. Maricalva Brun, M. Martyanov, S. Mazzoni, D. Medina Godoy, V. A. Minakov, J. Mitchell, J. C. Molendijk, J. T. Moody, M. Moreira, P. Muggli, E. Öz, C. Pasquino, A. Pardons, F. Peña Asmus, K. Pepitone, A. Perera, A. Petrenko, S. Pitman, A. Pukhov, S. Rey, K. Rieger, H. Ruhl, J. S. Schmidt, I. A. Shalimova, P. Sherwood, L. O. Silva, L. Soby, A. P. Sosedkin, R. Speroni, R. I. Spitsyn, P. V. Tuev, M. Turner, F. Velotti, L. Verra, V. A. Verzilov, J. Vieira, C. P. Welsch, B. Williamson, M. Wing, B. Woolley, and G. Xia. Acceleration of electrons in the plasma wakefield of a proton bunch. *Nature*, 561(7723):363–367, 2018.
- [15] G Schrgder, U Jansson, R Jung, G R Stevenson, and E B Vossenberg. The LEP Beam Dumping System. pages 2429–2431.
- [16] Polepalle Satyamurthy, Pravin Rai, Vikas Tiwari, Kiran Kulkarni, John Amann, Raymond G. Arnold, Dieter Walz, Andrei Seryi, Tristan Davenne, Ottone Caretta, Chris Densham, and Robert B. Appleby. Design of an 18 MW vortex flow water beam dump for 500 GeV electrons/positrons of an international linear collider. *Nuclear Instruments and Methods in Physics Research, Section A: Accelerators, Spectrometers, Detectors and Associated Equipment*, 679:67–81, 2012.
- [17] D Schumann, J Neuhausen, J Eikenberg, M Rüthi, M Wohlmuther, P W Kubik, H.-A Synal, V Alfimov, G Korschinek, G Rugel, and Th Faestermann. Radiochemical analysis of a copper beam dump irradiated with high-energetic protons. *Radiochim. Acta*, 97:123–131, 2009.
- [18] A Leuschner and K Tesch. The residual radioactivity of a water-copper beam dump for the TESLA Test Facility. Technical report, 1998.
- [19] H. C. Wu, T. Tajima, D. Habs, A. W. Chao, and J. Meyer-ter Vehn. Collective deceleration: Toward a compact beam dump. *Physical Review Special Topics - Accelerators and Beams*, 13(10):1–8, 2010.
- [20] Kieran Hanahoe, Guoxing Xia, Mohammad Islam, Yangmei Li, Öznur Mete-Apsimon, Bernhard Hidding, and Jonathan Smith. Simulation study of a passive plasma beam dump using varying plasma density. *Physics of Plasmas*, 24(2), 2017.
- [21] A. Bonatto, C. B. Schroeder, J. L. Vay, C. G.R. Geddes, C. Benedetti, E. Esarey, and W. P. Leemans. Passive and active plasma deceleration for the compact disposal of electron beams. *Physics of Plasmas*, 22(8), 2015.
- [22] Alexander Pukhov. Particle-in-Cell Codes for plasma-based particle acceleration. 2015.
- [23] Alistair Lawrence-Douglas. Ionisation effects for laser-plasma interactions by particle-in-cell code. 2013.
- [24] K. Bennett. EPOCH Users Manual for the EPOCH PIC codes, Ver. 4.3.4. 2015.
- [25] Christopher Ridgers Chris BRADY, Keith BENNETT, Holger SCHMITZ. EPOCH: Extendable PIC Open Collaboration.
- [26] Hartmut Ruhl. Classical Particle Simulations with the PSC code. Technical report.
- [27] The Computational Shared Facility.

- [28] LANL. VisIt User ' s Manual. (October), 2005.
- [29] John M Dawson. Electron Oscillations in a Cold Plasma. Technical Report 2, 1959.
- [30] Spencer J Gessner. DEMONSTRATION OF THE HOLLOW CHANNEL PLASMA WAKE-FIELD ACCELERATOR A DISSERTATION SUBMITTED TO THE DEPARTMENT OF PHYSICS AND THE COMMITTEE ON GRADUATE STUDIES OF STANFORD UNIVERSITY IN PARTIAL FULFILLMENT OF THE REQUIREMENTS FOR THE DEGREE OF DOCTOR OF PHIL. Technical report, 2016.
- [31] John David Jackson. Jackson - Classical Electrodynamics (3rd Ed.).pdf, 1962.
- [32] T Katsouleas, S Wilks, P Chen, J M Dawson, and J J Su. BEAM LOADING IN PLASMA ACCELERATORS. Technical report, 1987.
- [33] S Vaganian and H Henke. THE PANOFSKY-WENZEL THEOREM AND GENERAL RELATIONS FOR THE WAKE POTENTIAL. Technical report, 1995.
- [34] Francesco Mira and Thesis Advisor. Self Injection of High Brightness electron beams via Wakefield Ionization in beam-driven Plasma Acceleration. (October), 2017.
- [35] A. Bonatto, C. B. Schroeder, J. L. Vay, C. R. Geddes, C. Benedetti, E. Esarey, and W. P. Leemans. Compact disposal of high-energy electron beams using passive or laser-driven plasma decelerating stage. *AIP Conference Proceedings*, 1777(1):0–5, 2016.
- [36] ACCELERATOR WITH EXCELLENCE IN APPLICATIONS.
- [37] P. A. Walker. HORIZON 2020 EuPRAXIA Design Study. *Journal of Physics: Conference Series*, 874:012029, 2017.
- [38] K Schmid and L Veisz. Supersonic gas jets for laser-plasma experiments. *Citation: Review of Scientific Instruments*, 83:53304, 2012.
- [39] A. R. Maier, A. Meseck, S. Reiche, C. B. Schroeder, T. Seggebrock, and F. Grüner. Demonstration Scheme for a Laser-Plasma-Driven Free-Electron Laser. *Physical Review X*, 2(3):031019, sep 2012.
- [40] C Huang, W Lu, M Zhou, C E Clayton, C Joshi, W B Mori, P Muggli, S Deng, E Oz, T Katsouleas, M J Hogan, I Blumenfeld, F J Decker, R Ischebeck, R H Iverson, N A Kirby, and D Walz. Hosing Instability in the Blow-Out Regime for Plasma-Wakefield Acceleration. 255001(December):1–4, 2007.
- [41] Brendan B Godfrey. Suppressing the Numerical Cherenkov Instability in FDTD PIC Codes. 2018.
- [42] Alexander Blinne, David Schinkel, Stephan Kuschel, and Nina Elkina. Maxwell Solvers.